Available online at www.sciencedirect.com
ScienceDirect
Journal of Nuclear Materials 363–365 (2007) 555–559
journal of nuclear materials
www.elsevier.com/locate/jnucmat

2-D mapping of ICRF-induced SOL perturbations in Tore Supra tokamak

L. Colas [a,*], J.P. Gunn [a], I. Nanobashvili [a], V. Petržílka [b], M. Goniche [a], A. Ekedahl [a], S. Heuraux [c], E. Joffrin [a], F. Saint-Laurent [a], C. Balorin [a], C. Lowry [a], V. Basiuk [a]

[a] *Association Euratom-CEA, CEA/DSM/DRFC, Centre de Cadarache, 13108 Saint-Paul Lez Durance, France*
[b] *Association Euratom/IPP.CR, Prague, Czech Republic*
[c] *LPMIA, UMR 7040 CNRS, BP 239 F-54506 Vandoeuvre cedex, France*

Abstract

ICRF-induced SOL modifications are mapped for the first time in 2-D around Tore Supra ICRF antennas using reciprocating Langmuir probes. When probe heads are magnetically connected to powered antennas, radical modifications of floating potentials V_{float}, effective temperatures T_{eff} and ion saturation currents are observed. V_{float} perturbations are located radially near antenna limiters, with a typical extension 2 cm. Poloidally they are locally minimal near the equatorial plane, and maximal near antenna box corners. Two possible interpretations for increased T_{eff} are proposed: localised electron heating and RF loop voltage induced along probe circuit. Both interpretations rely on the generation of parallel RF fields by parallel RF currents on the antenna structure. The topology of such currents could explain the 2-D structure of T_{eff} maps. Both interpretations also imply a positive DC biasing of the antenna environment. Differential biasing of nearby flux tubes drives DC $E \times B_0$ convection that could explain 2-D density patterns.

PACS: 52.40.Kh; 52.35.Mw; 52.40.Fd; 52.70.Ds; 52.50.Qt

Keywords: Biasing; ICRF; Particle drifts; Probes; Tore Supra

1. Introduction

The edge plasma environment of radio-frequency (RF) wave launchers is crucial for their own proper operation (wave coupling, heat loads on antenna front faces), but also for objects magnetically connected to them, as well as the overall Scrape-Off Layer (SOL) stability. Many indirect experimental indications suggest strong SOL modifications around powered Ion Cyclotron Range of Frequencies (ICRF) antennas [1–3]. More direct measurement allows quantifying SOL perturbations, with generally one-dimensional (1D) space resolution [4,11–13]. 2-D resolution transverse to magnetic field

* Corresponding author. Fax: +33 4 42 26 62 33.
E-mail address: laurent.colas@cea.fr (L. Colas).

0022-3115/$ - see front matter © 2007 Elsevier B.V. All rights reserved.
doi:10.1016/j.jnucmat.2006.12.052

lines is however required: RF-induced DC $E \times B_0$ convection is highly suspected [3,4], breaking the SOL natural poloidal symmetry. Moreover the spatial structure of SOL modifications is intimately linked with the topology of RF currents on the antenna structure [5,6]. 2-D information can thus help identifying detrimental elements of antenna design contributing to SOL modification. This paper presents and briefly discusses 2-D mappings for three edge plasma parameters around Tore Supra (TS) antennas using reciprocating Langmuir probes.

2. Experimental setup

The SOL is characterized with reciprocating double probes. Fig. 1 sketches their electrical circuit: a DC bias V_0 is imposed between two electrodes, and the DC current I flowing between them is measured. Here DC means 'with slow time variations over a RF period'. In practice V_0 is 'slowly' swept in time to produce DC electrical characteristics $I = f(V_0)$. The whole electrical circuit is floating with respect to the 'ground'. The small current i through a high impedance R yields absolute DC potential V_A. One electrical circuit of this type is present on each side of the probe. The ion side can be magnetically connected to ICRF antennas. The electron side is connected to the toroidal limiter *via* the high field side. Two probes are installed on TS upper ports.

ICRF antennas, shown on Fig. 2, consist of two radiating straps embedded in a metallic box, partially closed on the plasma side by a tilted Faraday Screen. Antisymmetric strap phasing $(0, \pi)$ was used, in D(H) minority heating at the RF frequency of 57 MHz. The antenna box is shadowed by CFC private limiters: field lines from Langmuir probes either hit side limiters or pass radially in front of the whole structure and connect further away. The antenna structure is mobile horizontally.

Depending on the edge safety factor $q(a)$, Langmuir probe 1 can be magnetically connected to either ICRF antenna Q1 or antenna Q2, and probe 2 to antenna Q5. Field lines from probe 2 are traced up to their strike point in the poloidal cross section containing the septum of antenna Q5 (see Fig. 2), with estimated centimeter scale precision. Magnetic ripple is taken into account. Connection points are labelled by their altitude Z_{Q5} and their radial distance δr to side limiters. 2-D mapping thus amounts to scanning $(\delta r, Z_{Q5})$. Radial resolution is provided by the probe reciprocation, while poloidal resolution is obtained by scanning $q(a)$ through plasma current steps. From shot to shot several ICRF antennas were combined, for three private power levels $(0, 1, 1.5$ MW/antenna) and two antenna horizontal positions. 950 kW Lower Hybrid (LH) power was added to extend plasma durations and provide LH coupling measurements.

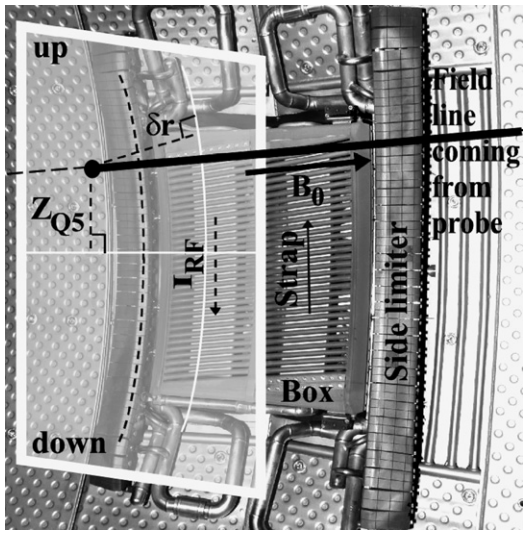

Fig. 2. ICRF antenna front face, and field line trajectory from probe to connection point $(\delta r, Z_{Q5})$ in the poloidal plane of antenna septum.

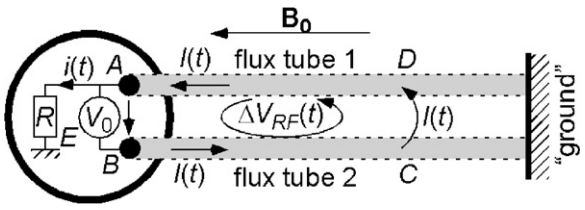

Fig. 1. Schematic of Langmuir probe electrical circuit, with RF-induced loop voltage $\Delta \tilde{V}_{RF}(t)$.

3. Experimental observations

3.1. Floating potential V_{float}

V_{float} is defined as $V_A = V_B$ when $V_0 = 0$ (see Fig. 1). Fig. 3 plots V_{float} versus δr during all plunges of probe 2 at $q(a) = 3.9$. For this safety factor and $\delta r = 0$, Z_{Q5} is -21 cm, i.e., field lines from the probe pass in front of the lower part of Q5 antenna. When antenna Q5 is passive (other antennas may be energized), V_{float} is slightly negative and slowly increases radially outwards. When antenna Q5 is powered localised high positive peaks of V_{float}

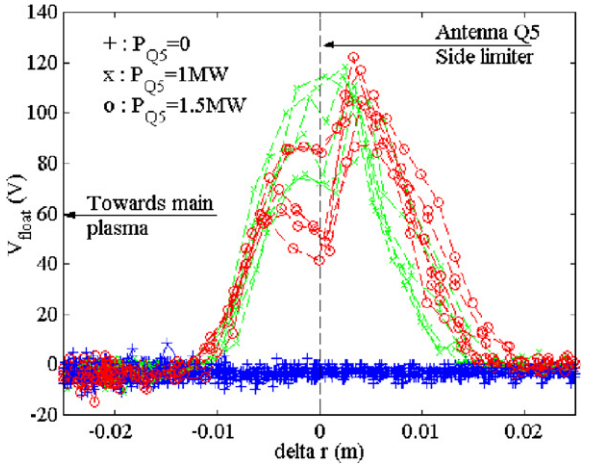

Fig. 3. V_{float} versus δr during all probe plunges at $q(a)$=3.9, connected side. $Z_{Q5} = -21$ cm for $\delta r = 0$.

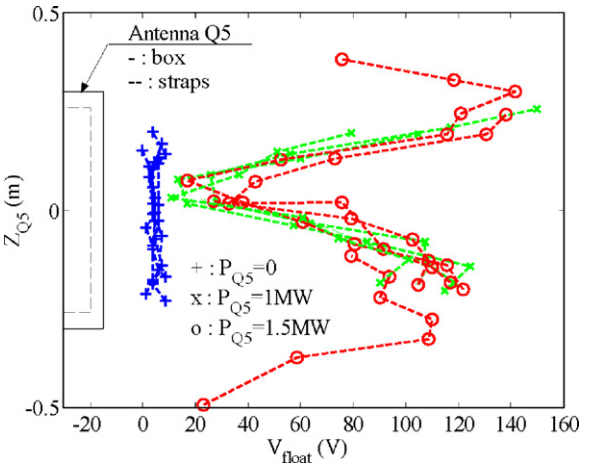

Fig. 4. Amplitude of local maxima of V_{float} in probe plunges, as a function of their altitude Z_{Q5}, connected side.

appear on the connected (ion) side of the probe, and smaller peaks on the unconnected (electron) side. Simultaneously, probe 1, connected to passive antennas, shows no perturbation. When $q(a)$ is changed the peak of V_{float} remains at the radial position of the side limiter within ±1 cm. When antenna Q5 is moved horizontally the peak is displaced consistently with the launching structure. This suggests a local RF effect due to the sole operation of Q5 antenna, and justifies the choice of $(\delta r, Z_{Q5})$ to map this 'ICRF-perturbed zone'.

Fig. 3 shows that the *ICRF-perturbed zone* is radially centered near the leading edge of side limiters on the connected side (a few mm in front of them on the unconnected side). The radial width of the *perturbed zone* is typically 2 cm on the connected side (1 cm on the unconnected side). This is only a few times larger than electrode dimensions (diameter 4 mm), so instrumental broadening may be at play. No clear difference in amplitude is observed between power levels $P_{Q5} = 1$ MW and 1.5 MW, whereas antenna front face temperature elevations scale as $P_{Q5}^{1/2}$ [1]. At high P_{Q5} a two-peak structure seems to emerge, particularly for high $|Z_{Q5}|$ on the connected side. It is not clear whether this reflects an intrinsic property of the SOL or an instrumental artefact.

Fig. 4 plots the amplitude of local V_{float} maxima versus Z_{Q5} over the scan of $q(a)$. The antenna vertical structure is also sketched. When antenna Q5 is passive, $|V_{\text{float}}|$ is low and poloidally homogeneous within the scatter of experimental points. However, when $P_{Q5} > 0$, V_{float} exhibits strong poloidal variation that is nearly symmetric with respect to the equatorial plane, with a local minimum observed near $Z_{Q5} = 0$, and local maxima near lower and upper parts of the antenna box.

Fig. 5 maps V_{float} as a function of $(\delta r, Z_{Q5})$ during two shots at $P_{Q5} = 1.5$ MW. Two structures of potential, radially centered near side limiters, clearly emerge on top and bottom of the antenna. Several probe–antenna pairs produce similar V_{float} patterns.

3.2. Ion saturation current J_{sat}

J_{sat} is defined as current I when $|V_0| > 180$ V (see Fig. 1). J_{sat} is representative of the local plasma density, provided that probe saturation is achieved. To eliminate global effects of $q(a)$ and additional power on the whole SOL, J_{sat} is normalised to its

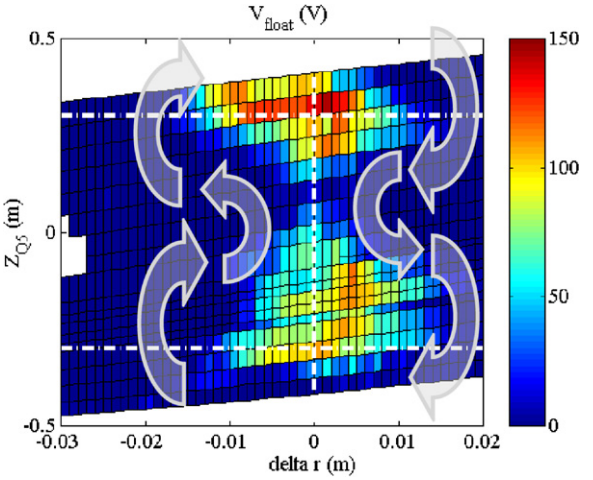

Fig. 5. 2-D map of V_{float} versus $(\delta r, Z_{Q5})$, connected side. Dashed lines: side limiter radial position, and antenna box vertical extension. Arrows: sketch of $v_{E\times B}$ induced by ∇V_{float}.

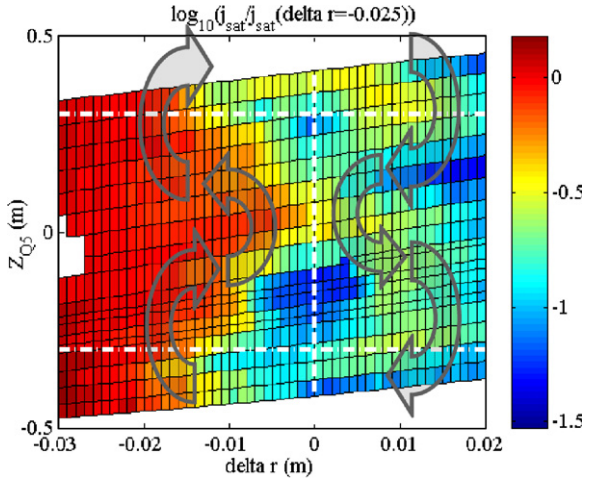

Fig. 6. 2-D map of normalized $J_{sat}/J_{sat}(\delta r = -0.025)$, connected side (log. scale). Dashed lines: side limiter radial position, and antenna box vertical extension. Arrows: sketch of $v_{E\times B}$ induced by ∇V_{float}.

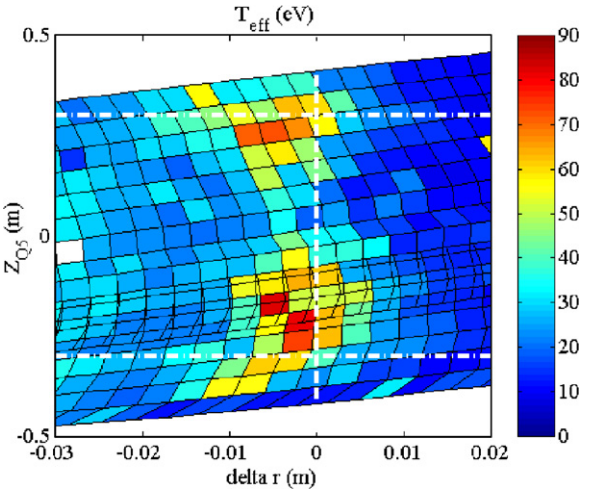

Fig. 7. 2-D map of T_{eff}, connected side. Dashed lines: side limiter radial position, and antenna box vertical extension.

value in $\delta r = -0.025$ m. On Fig. 6 normalized J_{sat} is mapped as a function of $(\delta r, Z_{Q5})$ during two shots at $P_{Q5} = 1.5$ MW. When antenna Q5 is passive, this map is poloidally homogeneous and exhibits a smooth radial decay with e-fold length $\lambda_j \sim 3$ cm. Outside the *ICRF-perturbed zone* the measured radial structure is similar with and without RF power on antenna Q5. In the *perturbed zone*, the radial variation strongly depends on Z_{Q5}. Near $Z_{Q5} = 0$ J_{sat} keeps its value without RF power, or even increases by 20% for $\delta r = -1$ cm. A 'current hole' appears near the bottom of the antenna, with J_{sat} reduced by 85%. Part, but not all this behaviour may be explained by a non saturation of the probe. The hole is radially centered near side limiters, with a typical radial extension 2 cm. Contrary to V_{float}, a stronger depletion is observed on the lower part of the antenna than on the upper part. Similar up-down asymmetry was obtained for hot spots [1,4]. Analysis of LH coupling over $q(a)$ scans, for six combinations of two LH grills and three ICRF antennas, also suggests localised ICRF influence on LH waveguides connected near upper and lower parts of antenna boxes. J_{sat} modifications are less pronounced on the unconnected side. No clear difference is observed between $P_{Q5} = 1$ MW and $P_{Q5} = 1.5$ MW.

3.3. Effective temperature T_{eff}

T_{eff} is extracted by fitting theoretical curves on measured double probe DC I–V_0 characteristics. Ion saturation is not always achieved in the strongly *perturbed zone*, where T_{eff} reaches half the maximum probe bias $V_{0max} = 200$ V. In addition I–V_0 characteristics sometimes depart from the expected $\tanh(eV_0/2T_{eff})$ shape. Several possible causes for this departure are: (a) non-thermal electrons; (b) plasma inhomogeneities between the two electrodes, spaced by 7 mm poloidally; (c) RF-induced changes of probe behaviour (see below). This explains the term 'effective' electron temperature.

Fig. 7 maps T_{eff} versus $(\delta r, Z_{Q5})$ during two shots at $P_{Q5} = 1.5$ MW. The pattern obtained is similar to that of V_{float}, with two zones of high T_{eff} centered near side limiters, 1 cm-wide radially, in the lower and upper parts of the antenna box. The main observations made for V_{float} also apply for T_{eff}, except no double peak is observed for T_{eff}.

4. Interpretation

Increased T_{eff} could indicate localized electron heating, e.g., by Landau damping in the near parallel RF field [6] or Fermi acceleration in oscillating RF sheaths [7,8]. Both of these processes should produce nonthermal electrons. An alternative explanation invokes an oscillating loop voltage $\Delta\widetilde{V}_{RF}(t) = -\frac{d}{dt}\int\int_{ABCD} B_{RF}(t)dS = \oint_{ABCD} E_{RF}(t)dl$ induced by RF slow waves along the probe electrical circuit (see Fig. 1). Physically $\Delta\widetilde{V}_{RF}(t)$ acts as a RF modulation of the DC bias V_0. Due to the non-linear sheath behaviour at probe electrodes, $\Delta\widetilde{V}_{RF}(t)$ can reduce the slopes of DC I–V_0 characteristics. T_{eff} is then larger than real temperatures, and provides an evaluation of $|\Delta\widetilde{V}_{RF}|$ when $e|\Delta\widetilde{V}_{RF}| \gg T_e$. Both above

interpretations rely on the generation of parallel RF fields by parallel RF currents on the antenna structure. With $(0,\pi)$ strap phasing, such RF currents are predicted near antenna box corners [5]. Other models yield similar results (e.g., [6]). In addition the radial width of the perturbed zone is of the order of the skin depth c/ω_{pe} for slow waves [5]. Both electron heating and RF-induced loop voltage also imply a positive DC biasing of the antenna environment [6–8]. This could be linked with measured positive V_{float}, since experimentally the regions with high potential coincide with those of high T_{eff}. Similar biasing was evidenced in front of LH launchers [9]. As sketched in Fig. 5, $E\times B_0$ drift across the gradient of V_{float} map produces two convective cells, with $v_{E\times B}$ directed upwards on the plasma side of the cells. Typical value $|\nabla V_{float}| \sim 10$ kV/m, inferred from Fig. 3, crossed with local $B_0 \sim 2.9$ T, yields $v_{E\times B} \sim 3.5$ km/s. Convection could explain localised modifications of J_{sat}, via the density: qualitatively iso-J_{sat} curves in Fig. 6 are close to stream lines of $E\times B_0$ flow. Density depletion in the upper and lower parts of TS antennas, with up–down asymmetries, was also predicted numerically [4].

5. Conclusions and prospects

Langmuir probes are powerful tools to characterize local RF-induced SOL modifications. The measurement technique however needs assessment in RF environments. This technique could be refined by using emissive probes to measure real plasma potentials, or a Retarding Field Analyser to evidence suprathermal particles. Mappings reveal RF-induced SOL patterns with an intrinsically 2-D structure strongly influenced by the antenna geometry. A Faraday screen with misalignment $<3.5°$ does not completely suppress these perturbations. RF-induced patterns extend radially over typically one skin depth for slow waves. Highest V_{float} and T_{eff} are found in lower and upper antenna parts. Several models predict such poloidal localisations [5,6]. In [5] this was attributed to toroidal RF currents near antenna box corners. Reduction of such parallel currents should thus be envisaged in future antenna designs. Interpretative theories [5,6] could be further assessed by changing the RF current distribution over antenna front faces. Mapping antennas in $(0,0)$ strap phasing, or the ITER-like TS antenna prototype, featuring a new electric scheme [10], would therefore be useful. J_{sat} 'holes' as well as over-densities are observed. Their 2-D structure seems compatible with convective transport in the map of ∇V_{float}. This needs confirmation by simulation. Density depletion could explain LH coupling modifications. Some observations still need interpretation: absolute values of T_{eff} and V_{float}, double peaks of V_{float}. The scaling of V_{float} with P_{Q5} contradicts the parametric dependence of hot spot temperature elevation ($\propto P_{Q5}^{1/2}$ [1]). Low power experiments could evidence a possible saturation of RF non-linear mechanisms and provide better measurements with good probe saturation even in the *perturbed zone*.

Acknowledgement

One of the authors (V. Petržílka) was supported in part by the Czech Grant project GACR 202/04/0360.

References

[1] L. Colas et al., Nucl. Fusion 46 (7) (2006) S500.
[2] A. Ekedahl et al., 15th Topical RF Conf., Moran AIP CP 694 (2003) 259.
[3] D.A. D'Ippolito, J.R. Myra, et al., Phys. Fluids B 5 (10) (1993) 3603.
[4] M. Bécoulet et al., Phys. Plasmas 9 (6) (2002) 2619.
[5] L. Colas, S. Heuraux, S. Brémond, G. Bosia, Nucl. Fusion 45 (2005) 767.
[6] V. Petrzilka et al., 22nd EPS Conf. Plasma Phys. 29C (2005) 2.095 (ECA).
[7] M.A. Lieberman, V.A. Godyak, IEEE Trans. Plasma Sci. 26 (1998) 955.
[8] M.D. Carter et al., Phys. Fluids B 4 (5) (1992) 1081.
[9] F. Jacek, V. Petrzilka, M. Goniche, PPCF 47 (2005) L17, No. 7.
[10] G. Bosia, Fusion Sci. Technol. 43 (2003) 153.
[11] G.R. Hanson, et al., in: Proc. of 11th Topical RF Conf., Palm Springs, 1995, p. 463.
[12] J.-M. Noterdaeme et al., 23th EPS Conf. Plasma Phys., Kiev (1997) 723.
[13] G. Van Oost et al., Fusion Eng. Des. 12 (1990) 149.